ISSN (O): 2320-5407
ISSN (P): 3107-4928
Journal Homepage: -www.journalijar.com
INTERNATIONAL JOURNAL OF ADVANCED RESEARCH (IJAR)
Article DOI:10.21474/IJAR01/24074
DOI URL: http://dx.doi.org/10.21474/IJAR01/24074

RESEARCH ARTICLE

TECTONIC STRUCTURES AND METAMORPHIC FACIES CHARACTERIZATION OF THE PAN-AFRICAN SOUTHERN OUADDAÏ MASSIF (EASTERN CHAD): CONSTRAINTS FROM FIELD OBSERVATIONS, MICROSTRUCTURES AND MINERAL CHEMISTRY

Malik Hisseine Malik[1], Félix Nenadji Djerossem[2], Moussa Isseini[3], Gilbert François NgonNgon[4],Issaka Ousman Al-Gadam[3] and Akumbom Vishiti[4,5]

1. University Polytechnic of Mongo, Department of Mining and Geology, BP: 4377 Mongo, Chad.
2. Iriba National Higher Institute of the Sahara and Sahel, Department of Mining, New and Renewable Energies, Chad.
3. University of N'Djamena, Department of Geology, Faculty of Exact and Applied Sciences of Farcha, BP: 1027 Chad.
4. Laboratory of Geosciences, Natural Resources and Environment, Faculty of Sciences, University of Douala. P.O. Box 24155 Douala, Cameroon.
5. Department of Civil Engineering, The University Institute of Technology (IUT), University of Douala, P.O. Box 8698, Douala, Cameroon.

Manuscript Info

Manuscript History
Received: 18 June 2026
Final Accepted: 20 July 2026
Published: August 2026

Key words:-
metasediments, tectono-metamorphic, Pan-African orogen, Southern Ouaddaï massif, Chad.

Abstract

The Pan-African Southern Ouaddaï Massif (eastern Chad) records a polyphase tectono-metamorphic evolution involving three successive deformation stages. An initial regional foliation (D1) is expressed by composite S0/S1 surfaces oriented NE–SW to NW–SE with shallow to moderate dips, reflecting NW–SE shortening. The most pervasive phase (D2) is defined by S2 schistosity transposing earlier fabrics into S0/S1-2, associated with isoclinal folds (F1, F2), gently plunging lineations (L1, L2), and dextral mylonitic shear zones. Syn-D2 emplacement of muscovite-bearing leucogranites within shear zones highlights the contemporaneity of magmatism and deformation. A late-stage event (D3) corresponds to weakly developed axial-plane schistosity (S3), trending ENE–NE with steep dips, and is accompanied by brittle deformation expressed by NE–SW fracture networks locally filled with aplitic and pegmatitic veins.Metamorphic assemblages reveal a retrograde evolution from upper amphibolite facies (almandine garnet, biotite) to greenschist facies (quartz, muscovite, biotite, albite), with low-grade chlorite–sericite–actinolite–epidote associations preserved in the NW sector.

Corresponding Author:- Malik Hisseine Malik
Address:-University Polytechnic of Mongo, Department of Mining and Geology, BP: 4377 Mongo, Chad.

Collectively, these features document a complex tectono-metamorphic history dominated by NW–SE shortening, subsequent transpression, and late brittle fracturing, reflecting the dynamic evolution of the Pan-African orogen in eastern Chad.

Introduction:-

The Central African Pan-African Orogenic Belt (CAFB) is located between the Congo Craton in the south, the West African Craton in the west and the Sahara metacraton in the north (Figure 1a) [1] The CAFB outcrops in eastern Nigeria, Chad, Cameroon, Central African Republic and Sudan (Figure 1c)[2,3, 4,5, 6]. It is a large portion of a complex that includes the Pan-African Central African Tectonic Belts, the NE Brazil Belts and the Pan-African Trans-Saharan Chain [7,8,5,9, 10]. It continues eastwards into Sudan, Uganda and Tanzania [11]. This domain corresponds to the Central African Belt [12] which was formed during the convergence of the West African craton, the Congo and São Francisco cratons, and the Latea and Saharan metacratons [13, 1,14, 15]. The Central African Fold Belt (CAFB) was formed during the Pan-African orogeny (~600 Ma) through juvenile crustal rock formations and/ or by the intensive reworking of the pre-Pan-African basement [16].In Chad, the Central African Fold Belt is divided into five small massifs: the Tibesti massif in the north, the Guera massif in the center, the Mayo Kebbi massif in the south-west, the Mbaïbokoum massif in the south and the Ouaddaï massif in the east. Our study area, located to the south of the Ouaddaï massif, is dominatedby metasedimentary rocks and intruded by syn- to post-tectonic granites between 635 and 540 Ma [17, 18].

The Ouaddaï Massif is not well known geologically, which is why some authors attribute it to the Pan-African orogenic belt of Central Africa [12, 3,19], others consider that it corresponds to the reworked southern edge of the Archean to Paleoproterozoic Saharan metacraton (Figure 1c)[1, 20, 21, 22]and others proposing that it consists mainly of Neoproterozoic magmatic and sedimentary rocks [18, 23].The metamorphism and tectonic structures of the metasedimentary rocks are poorly defined in this study area. In this paper, we present issuesfrom field observations, microstructures and mineral chemistry ofmetasedimentary rocks to identify the tectonic structures and the degree metamorphism of the southern Ouaddaï Massif. At the end of the paper, we compare the deformation phases of the metamorphism with those of Cameroon and the Central African Republic, with the aim of understanding the tectono-metamorphic evolution in this portion of the crust.

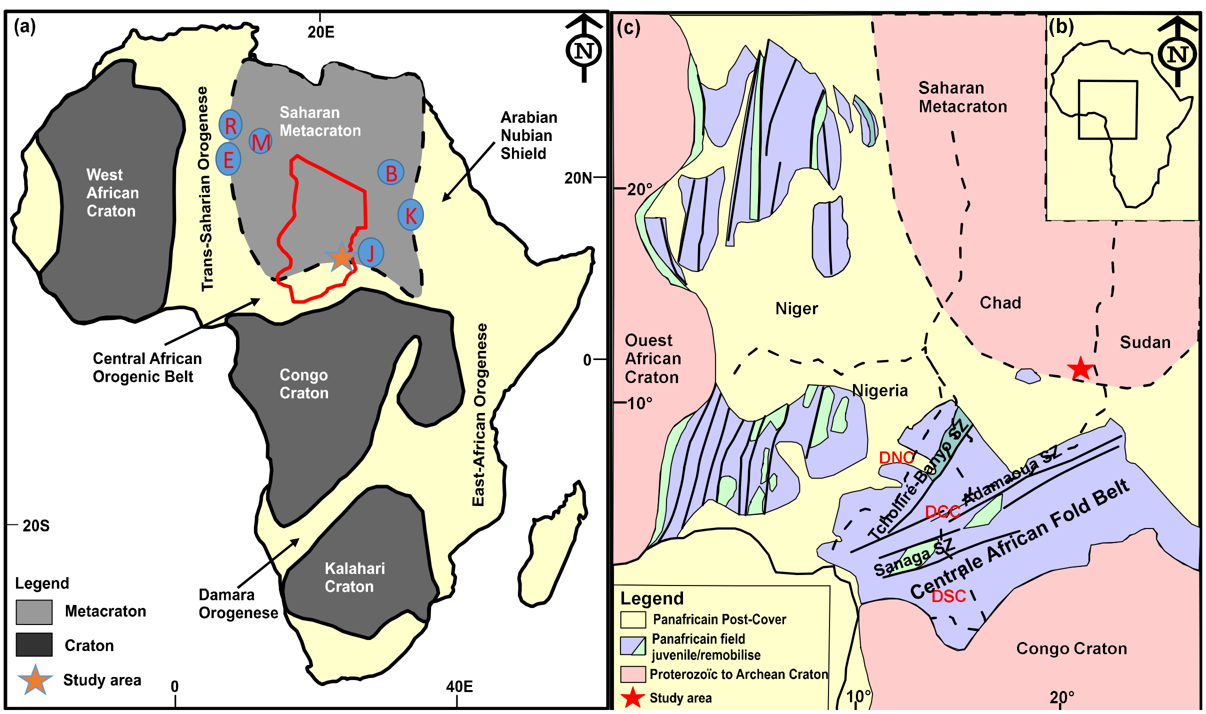

Figure 1

Figure 1. a) African Precambrian orogenic belts, metacraton and craton modified from[24,25]. B = Bayuda; J = Jebel Mara; R = Raghane Shear Zone; K = Keraf-Kabus-Sekerr Suture; M = Murzuk Craton; E = East Hoggar. (b) Map of Africa. (c) Map showing the position of the Central African orogenic belt and the remobilised/juvenile terrains modified from [3, 26].

Geological setting:-

The Ouaddaï massif is the largest Precambrian outcrop in Chad. It extends over more than 500 km from north to south, extends into Darfur (Sudan) and forms the eastern limit of the Chadian basin. It is essentially made up dominated by migmatitic and plutonic rocks in the northern Ouaddaï and made of lower grade metasedimentary rocks intruded by granodioritic to leucogranitic plutons a southern Ouaddaï (Figure 2a)[27, 17].

According to the work of[17], the geodynamic history of the southern part of the Ouaddaï Massif can be summarised by the opening of a rift with the emplacement of sedimentary series resulting from the erosion of cratons and the production of basic magmas (amphibolite) from the depleted mantle, probably attributed to a phase of crustal thinning associated with the D1 and D2 deformation. In addition to this evolution, (i) partial melting of the enriched mantle generating the pyroxene-biotite-monzonite granodiorite-granite series and (ii) crustal melting producing anatexis granites (biotite leucogranites and muscovite leucogranites). The intrusive rocks are calc-alkaline granites and granodiorites, often concordant with the metamorphic formations. This assemblage of intrusive rocks forms a large calc-alkaline batholith assigned to the Pan-African (Figure 2)[28, 17]. A few seams of rhyolites, dolerites, quartz and microgranites cross the batholith. The granites give Pan-African ages: 538 ± 5 Ma and 540 Ma (U-Pb on zircon) [29; 17](Figure 2a). [17]found Pan-African U-Pb zircon crystallization agesfrom two distinct post-tectonic granites (538 ± 5Ma and 540Ma) and reported the presence of detrital zircon grains with Hf isotopic signatures including Archean to Paleoproterozoic inherited components indicating that the metasedimentary rocks are derived from the erosion of neighbouring cratons.

Sampling and analytical methods:-

Field mapping and sampling:-

About twenty (20) samples were collected from the metasedimentary rocks of the Southern Ouaddaï Massif for petrography study and thin section were prepared at GeoRessources Laboratory. Petrographic studies together with quantitative modal analysis were carried out in order to characterize the minerals component of the rocks.The samples contain mineral assemblages and textures useful for tectonic and metamorphic characterization. The microstructural analysis was carried out on thin section using the document for [30]. Thirteen (13) key samples representative of the distinct lithologies are listed in table 1 with their location and mineral assemblages.

Electron microprobe:-

These samples were analyzed and the chemical compositions of some index minerals determined. Analyzes were conducted using a Cameca SX100 electron microprobe equipped with five (5) wavelength-dispersive spectrometers (WDS) at the Service Commun de Microscopies Electroniques et de Microanalyses X (SCMEM) in the GeoRessources laboratory (University of Lorraine) of Vandœuvre-lès-Nancy (France). The thin polished slides were coated with a thin layer of carbon at around 50µm using an Edwards carbon evaporator (type auto 306). Backscattered electron (BSE) imaging, and chemical analysis on the thin section metasediments were obtained using a CAMECA SX100 electron microprobe operated at 20 kV and 40 nA at the SCMEM of Nancy, France.The accelerating voltage was 15kv and the counting 10s on peak[31]. A single program was used for all the silicates. The structural formula for micas, plagioclases, epidotes, amphiboles, pyroxenes, garnets and staurolites were calculated respectively on the basis of 22 (O), 8 (O), 12,5 (O), 23 (O), 6 (O), 12 (O) and 46 (O) after [32].

Table 1. Description and location of the investigated samples.

Samples	Latitude	Longitude	Lithology	Mineralogical assembly
F03a-18b	12°13’01,7’’	21°57’06,7’’	Garnet-Micaschist	Grt + Bt + Pl + Mus + Qtz
F04a-18	12°13’15,5’’	21°56’50,4’’	Staurolite-Micaschist	Bt + Grt + St + Mus + Qtz
F06b-18	12°13’37,8’’	21°55’22,3’’	Calc-silicate gneisses	Hbl + Grt + Pl + Px + Kfs + Cal + Qtz
AB06a-19	12°25’09,7’’	21°08’28,6’’	Micaschist	Bt + Phg + Qtz
AB14-19	12°27’13,9’’	21°19’25,8’’	Micaschist	Bt + Kfs + Mus + Qtz
AB15-19	12°28’41,3’’	21°21’47,7’’	Greenschist	Chl + Ser + Ep + Qtz
F11-18	12°12’29,8’’	21°51’42,3’’	White granit	Bt + Mus + Qtz+ Pl + Kfs
F12-18	12°11’40’’	21°50’46,8’’	White granit	Bt + Mus + Qtz+ Pl + Kfs
F13b-18	12°11’08,8’’	21°51’06,4’’	White granit	Bt + Mus + Qtz+ Pl + Kfs
F13c-18	12°11’08,8’’	21°51’06,4’’	Diorite	Bt + Mus + Qtz+ Amp +Pl
AB19a-19	12°26’18,7’’	21°26’33,1’’	Biotite-granit	Bt + Mus + Qtz+ Amp + Kfs

AB19b-19	12°26’18,7’’	21°26’33,1’’	Granodiorite	Bt + Mus + Qtz +Pl
AB21b-19	12°11’36,6’’	21°23’56,9’’	Quartzite	Qtz +Pl+ Mus

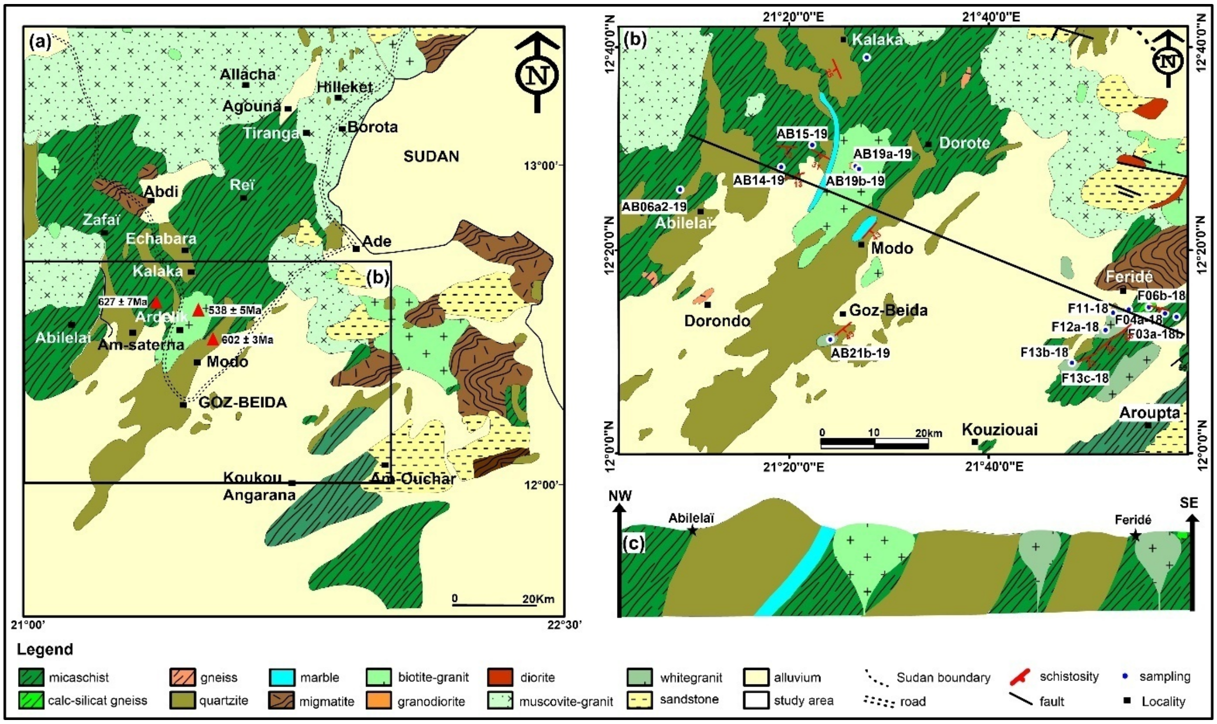

Figure 2

Figure 2. (a) Geological map of the Southern Ouaddaï modified from [33], ages of quartzite, metapelites and biotite granite are highlighted by[17].(b) Geological map showing localities included in the study area and the geographical position of the samples studied modified after [27,17].(c) Geological cross-section of the study area.

Result:-

Petrography of themetasedimentary rocks:-

Chlorite-sericite-epidote-quartz greenschist:-

The greenschist occurs as a flake (Figure3a) and is generally oriented. The chloritoschist belongs to the greenschist facies due to the presence of minerals such as actinote, epidote etc.... It is strongly schistose and metamorphosed with a protomylonite texture. The average schistosity measurements are N50E and a dip of 35 to the NW. They are greenish in colour. The mineralogical assemblage is: quartz, chlorite, epidote, sericite.... Quartz (60 to 70%) occurs as fine grains in the rock or as stretched phenocrysts. It has a rolling extinction with zones of dynamic recrystallisation (Figure3b). The new grains created are very small and have equant boundaries, forming a so-called core-and-mantle structure[30]. Sericite (5-10%) is very fine-grained and fibrous in appearance. Chlorites (2 to 5%) are fibrous, very fine due to the deformation. They are authentic minerals. They can also come from the diagenetic or anchi metamorphic recrystallisation of clays of the smectite group. Actinotes (10-20%) are light green in colour and occur as elongated prisms up to 3mm in length (Figure3c). Oxides are also observed as opaques.

Biotite-muscovite-garnet micaschist:-

The Garnet micaschist outcrops in relief, in the form of flakes and sheets showing a schistosity which is pushed, intersected by quartz veins (Figure3d). The schistosity is generally oriented N40E 50SE. And not far from Feridé, the rock outcrops all along the stream, in sheets showing schistosity, with much muscovite visible to the naked eye. The average schistosity is oriented N35E 35SE. The rock is intersected by a quartz vein running N35E 30SE. Microscopically, the rock has a heterogranular lepidoblastic texture and a microfoliation where micas and quartz veins alternate. The rock is composed of quartz, feldspar, micas and garnet. Quartz grains (30 to 40%) are xenomorphic, stretched out underlining the schistosity and present a rolling extinction and of size going from 0.1 to 0.6mm on 0.1 to 0.4mm of width. Micas (30-40%) form elongated crystals 0.15-0.8mm in diameter. They are found embedded in garnet porhyroblasts. Two generations of micas are identified: the micas outlined by the S1 schistosity are intersected by garnet (Figure3e). And a second generation which is embedded in the garnets (Figure3f). Plagioclase (5-10%) (Figure3e) occurs as automorphic to subautomorphic crystals of variable size, the plagioclase sections are generally provided with polysynthetic macles. They are deformed and have fractures within the mineral. Garnet (5-10%) is highly altered, with numerous quartz inclusions. It occurs as idiomorphic porphyroblasts of variable size (2 to 5 mm), often cracked and containing quartz and mica inclusions. The garnet is surrounded by biotite, muscovite and quartz.

Biotite-muscovite-garnet-staurotide micaschist:-
In the Feridé zone, to the SE of the study area, the garnet micaschists are very deformed. They occur along the entire length of the watercourse, in sheets with schistosity, with much muscovite and garnet visible to the naked eye. The average schistosity is oriented N35E 35SE. The rock is intersected by a quartz vein trending N35E 30SE (Figure3g). Microscopically, the rock F04a-18 has a heterogranular oriented lepidoblastic texture and microfoliation with alternating micas and quartz veins. The rock is composed of quartz, feldspar, biotite, muscovite and garnet. Quartz grains (30-40%) are xenomorphic, stretched, emphasizing the schistosity and show a rolling extinction and size ranging from 0.1 to 0.6mm by 0.1 to 0.4mm in width. Micas represent about 20 to 30% of the rock and are present in the form of stretched and oriented flakes with muscovite being dominant. Garnet (5 to 10%) is highly altered and has numerous quartz inclusions. The micaschists are enriched with garnets and a new mineral, staurotide. The staurotide porphyroblast is elongated and cracked, bent and rotated and this provides evidence of crystallization during late metamorphism. It is rusty brown in specimen with low pleochroism, high relief and straight extinction in thin section (Figure3h, i). Its low abundance, xenomorphic habitus and highly recrystallized matrix confound textural observations that might have allowed the staurolite to be located in relation to deformation episodes. Staurotides are particularly abundant in pelitic levels [34]. The sillimanite is also observed in this thin section at the micaschist (Figure 3h, i).

Garnet–amphibole-pyroxene-calcite gneisses:-
The calc silicate gneiss outcrops in banks and blocks not far from the village Feridé. It is in partial contact with the outcrops of the garnet mica schists at the base. It is dark in colour, showing a foliation with alternating dark (ferromagnesian) and light (quartz and feldspar) beds with posterior garnets(Figure3j).

Microscopic observation of sample F06b-18 (Figure3k, l) shows a mineral association composed of quartz, feldspar, hornblende, calcite, pyroxene.... Quartz (20-30%) is xenomorphic and shows dynamic recrystallisation. Feldspar (15 to 20%) composed of plagioclase and orthoclase is automorphic to subautomorphic in the form of a beach. Hornblende (15 to 20%) is abundant in the rock, greenish in colour and sometimes associated with pyroxene. Pyroxene (2 to 5%) is automorphic to subautomorphic, stretched and sometimes has an amphibole halo. Garnet (15 to 20%) is abundant in the rock. It is later than the other minerals, cracked with calcite inclusions which explains the evolutionary history of garnet. The accessory minerals found are calcite, sphene, zircon.... Calcite (3 to 5%) is late, it fills in the gaps between the minerals. The texture of the rock is heterogranular lepidoblastic.

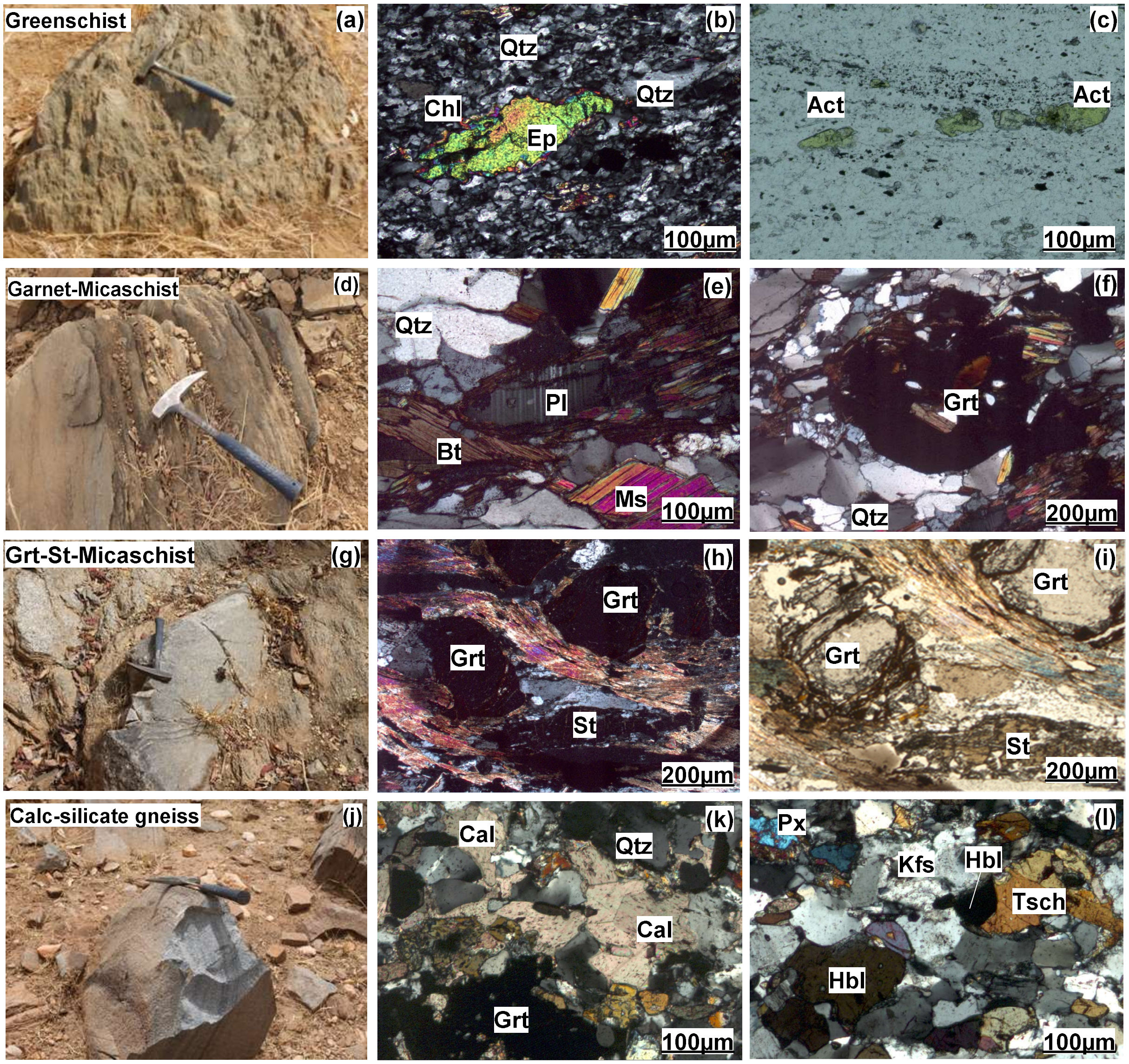

Figure 3. Photography and microphotography of metamorphic rocks.(a) Greenschist photography near Ardelik. (b), (c) Microphotograph of a mineralogical assemblage of chlorite, sericite, epidote, actinote and quartz in LPA. (d) Outcrop of garnet micaschist in sheet form, (e) Biotite + muscovite + plagioclase + quartz assemblage. (f) Garnet porphyroblast with biotite and quartz inclusion. (g) Quartz vein cut micaschist outcrop, (h) and (i) biotite + muscovite + garnet + staurolite + sillimanite in LPA and LNPA (j)Outcrop of calc-silicate gneisses in block form, (k) Calcite in association with Quartz. (l) Thin section showing the hornblende passage in tschermakite in analyzed and non-analyzed polarized light.

Deformation and tectonic structures:-According to field reports and microstructural analyses of the southern part of the Ouaddaï massif, three deformation phases have been identified. These of deformation phases are observed in the metasedimentary rocks, but also in the muscovite leucogranites, which are "concordant" with the latter.

Initial deformation phase D1:-The first deformation phase, D1, is observed within the metasedimentary rock units and corresponds to a composite S0/S1-type foliation, bounded by an extensive structure that is both horizontal and gently dipping, with average strike and dip directions of N120E and 15SW, respectively. In this picture (Figure 4a), the S0/S1 structure is marked by dark and light layers. This foliation is overlaid by the S2 schistosity, characterized by the elongation of biotite, feldspar, and even quartz crystals, and the arrangement of the minerals in sheets. Together, these two structures form an S0/S1-2 structure in the same picture(Figure 4a). The average strike of S0/S1 is NE-SW but it includes large variations from N-S to ENE-WSW. S0/S1 planes bear L1 lineations that plunge along the dip direction, hence suggesting folding of early tabular surfaces under NW-SE shortening without significant along strike movement.

Second deformation phase D2:-The second deformation phase is the most intense in our study area. It is marked by S2 schistosity, characterised by a preferential orientation of the feldspar minerals and the flake-like arrangement of the micas. Locally, it transposes the S0/S1 foliation. It trends NE-SW or NNE-SSW, dipping slightly to steeply to the NW or ESE.This S0/S1 surfaces are intersected by steep NNE-SSW to NE-SW shear zones that produced the crenulation of the previous structures (Figure4h). In this picture (Figure 4d), there is a mineral stretch line associated with S2 that dips slightly toward the NW. The tip of the pen, shown in light green, points toward the NW. At the macroscopic scale, the sense of shearing is uneasy to identify due to intense mylonitic deformation. However, it is recognizable at thin section observations and follow a dextral sense. Several muscovite bearing leucogranite occur within or in the vicinity of these D2 shear zones (Figure4h), crosscutting or transposed by the S2 planes (Figure4g, h), indicating a syn-D2 emplacement of the leucogranitic rocks within the shear zones. L2, when observed, lye between the strike and the dip direction of S2. The last tectonic structure identified in the second deformation phase corresponds to the asymmetric folds P2 resulting from the transposition of the S0/S1 foliation.

Third deformation phase D3:-The third deformation phase observed in our study area corresponds to a weakly expressed ENE or NE trending S3 axial plane schistosity, dipping steeply to the NW or NNW. This deformation phase is associated with several families of brittle deformation, characterized by dry joints and joints filled by magmatic material in the form of aplitic and pegmatitic veins trending predominantly NE-SW.

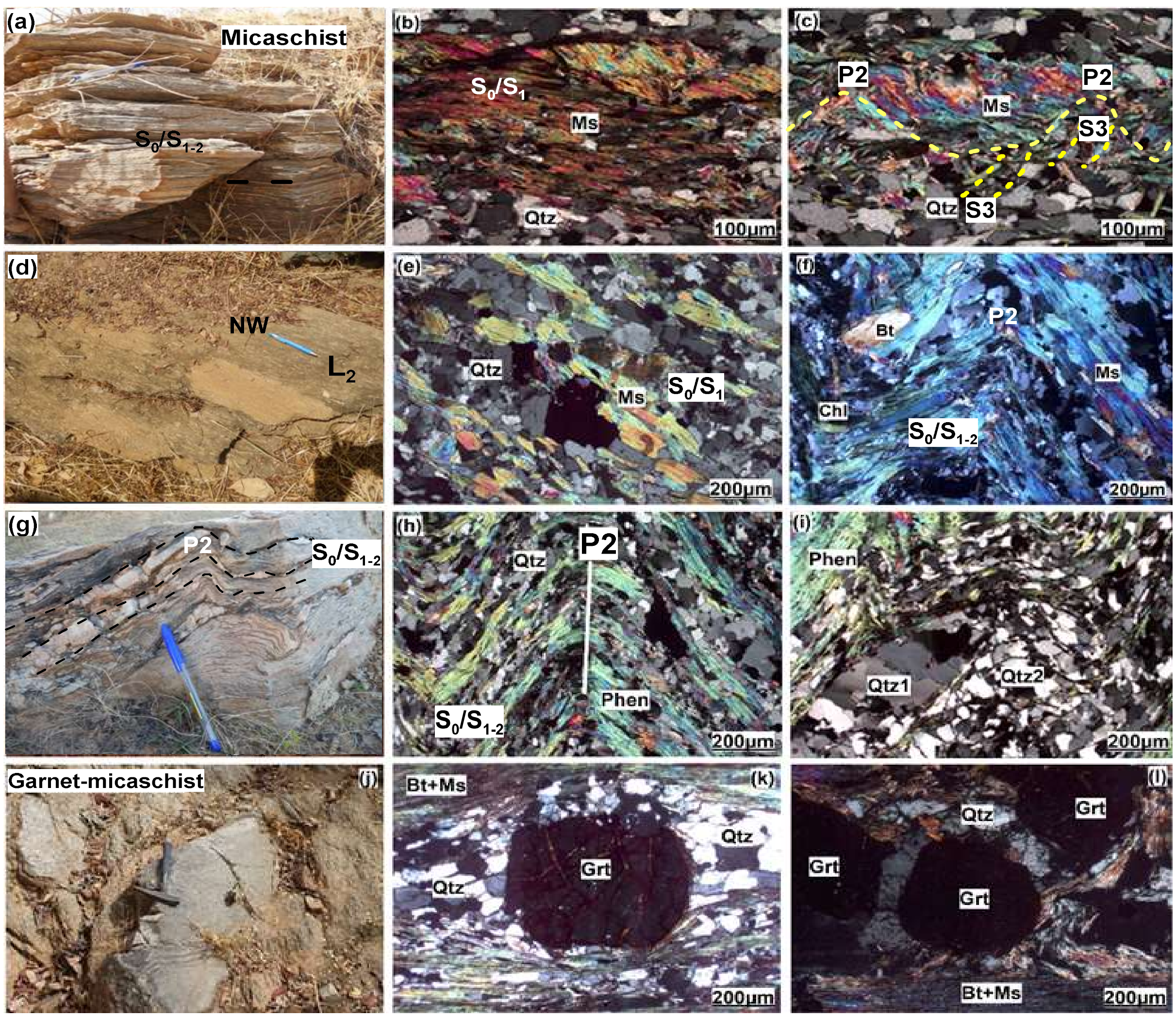

Figure 4. (a) Outcrops showing F1 and S0/S1 affecting quartzite and micaschist layers. (b) Thin section showing the micaceous quartzite. (c) D2 shear zone showing a transposed leucogranite and F2 folds. (e) Folded micaschist outcrop. (d) S2 crenulation affecting S0/S1 under the microscope. Mus = muscovite. Chl = chlorite. Bt = biotite.
(j) Outcrop of garnet micaschist in sheet form.(k)texture of foliated muscovites between quartz grains, pressure shadows around the garnet porphyroblast.(l) microphotograph showing the garnet posterior and mica.

Interpretation of the poles of the S1 and S2 schistosity planes:-

The stereogram in the figure shows a concentration of the poles of the S1 schistosity of the micaschists of the southern Ouaddaï massif towards the center (Figure 5a). This indicates relatively shallow dip angles (23°-24° on average). The figure also shows two preferred directions for S1 pole swarms, namely NE-SW and NW-SE. Both directions are dominant when the direction of the rosettes is observed (Figure 5c).

The figure shows a cluster of S2 schistosity poles concentrated towards the periphery of the stereogram's great circle, reflecting the greater dip angles (66-67° on average) (Figure 5b). These groupings of S2 poles define a dominant ENE-WSW direction. The rosette of directions (Figure5d) confirms this.

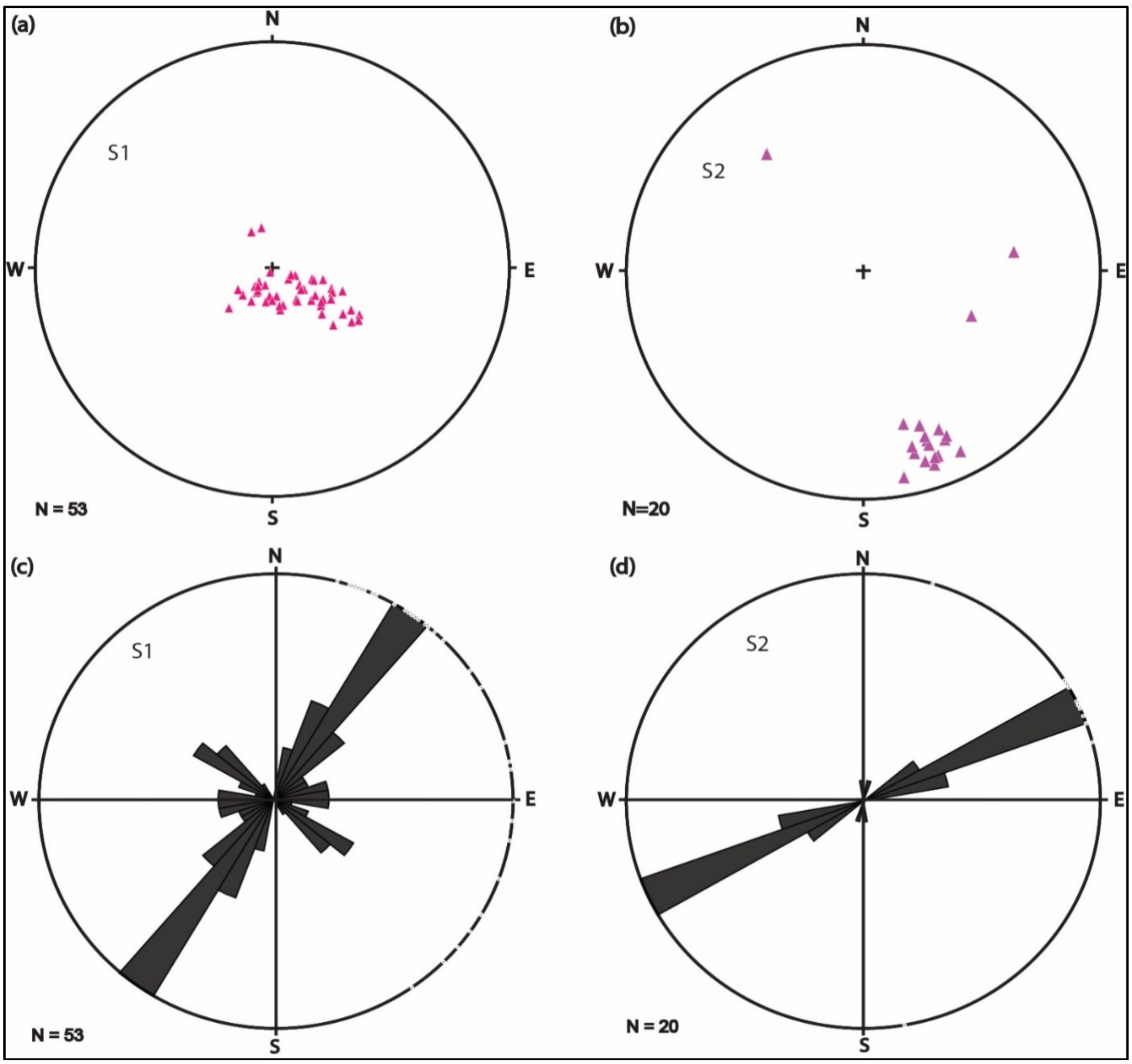

Figure 5. (a) and (b) Distribution of S1 and S2 schistosity poles in the metamorphic rocks (metasediments) of the southern Ouaddaï massif. (c) and (d) Distribution of S1 and S2 schistosity direction rosettes.

Silicate geochemistry:-

Mineral phase analysis:-

These mineralogical analyses make it possible to characterize the chemistry of the mineral phases of the metasediments.

Biotite:-

Biotites have varied Mg content in moles ranging from X_{Mg} (Mg/Mg+Fe) = 0.3-0.4 in sample F03a-18b through and their titanium content per formula unit (pfu) falls within 0.2 and 1.0 pfu (See Table 2). The biotites analyzed with the microprobe(Table 2) come from garnet micachists (F03a-18b). The ratio (Fe^{2+}/ Fe^{2+}+Mg) is between 0.4 and 0.60, which explainswhy these biotites are rich in iron (Figure 6b) and rich in TiO2 and MgO. Si values range from 5.5 to 5.7, the biotites fall between the siderophyllite and annite field (Figure 6a).

Table 2.Representative electron microprobe analyses of biotite. Structural formulas calculated on the basis of 22 oxygen anions. Note biotite in micaschist of garnet (analysis 13). C: cercle

Rock type	Micaschistes of Garnet									
Sample	F03a-18b									
Analysis	C2b-3	C3d-1	C3d-2	C3d-3	C4c-1	C5c-1	C5c-2	C1d-3	C1d-4	C5b-2
SiO_2	36,45	36,24	34,66	35,87	36,27	35,20	36,23	35,12	35,20	34,72
Al_2O_3	16,99	17,25	16,75	17,21	18,43	18,04	17,63	19,67	19,36	18,58
TiO_2	2,75	2,56	2,38	2,49	1,59	2,39	2,90	1,28	1,48	1,39
FeO	19,52	20,86	22,57	20,77	19,32	20,85	19,81	19,90	19,03	19,57
MnO	0,21	0,22	0,16	0,18	0,23	0,09	0,14	0,00	0,03	0,03
MgO	6,98	6,33	6,12	6,07	6,92	6,62	6,64	8,24	8,76	8,40
CaO	0,17	0,10	0,14	0,17	0,07	0,06	0,07	0,26	0,37	0,35
Na_2O	0,05	0,02	0,06	0,14	0,08	0,36	0,04	0,22	0,29	0,22
K_2O	8,31	8,45	7,82	8,19	8,33	8,37	8,77	7,84	6,78	7,22
Total	**91,43**	**92,03**	**90,66**	**91,09**	**91,23**	**91,98**	**92,22**	**92,53**	**91,30**	**90,48**
Si	5,748	5,719	5,614	5,717	5,714	5,570	5,682	5,466	5,498	5,515
Al^{iv}	2,252	2,281	2,386	2,283	2,286	2,43	2,318	2,534	2,502	2,485
Al^{vi}	0,906	0,927	0,81	0,951	1,137	0,935	0,941	1,075	1,063	0,995
Altotal	3,158	3,208	3,196	3,234	3,423	3,365	3,259	3,609	3,565	3,480
Ti	0,326	0,304	0,290	0,298	0,188	0,284	0,342	0,150	0,174	0,166
Fe^{2+}	2,574	2,753	3,057	2,769	2,545	2,759	2,598	2,590	2,486	2,600
Fe^{3+}	0,000	0,000	0,000	0,000	0,000	0,000	0,000	0,000	0,000	0,000
Mn	0,028	0,029	0,022	0,024	0,031	0,012	0,019	0,000	0,004	0,004
Mg	1,640	1,489	1,477	1,442	1,625	1,561	1,552	1,911	2,039	1,989
Ca	0,029	0,017	0,024	0,029	0,012	0,010	0,012	0,043	0,062	0,060
Na	0,015	0,006	0,019	0,043	0,024	0,110	0,012	0,066	0,088	0,068
K	1,672	1,701	1,616	1,665	1,674	1,690	1,755	1,557	1,351	1,463
Total	**15,191**	**15,227**	**15,316**	**15,222**	**15,236**	**15,363**	**15,230**	**15,392**	**15,266**	**15,344**
Mg#	0,389	0,351	0,326	0,342	0,389	0,361	0,373	0,425	0,451	0,433
XFe	0,503	0,532	0,572	0,536	0,480	0,525	0,510	0,464	0,445	0,466
XAl	0,177	0,180	0,152	0,184	0,214	0,178	0,185	0,193	0,190	0,178
XMg	0,320	0,288	0,276	0,280	0,306	0,297	0,305	0,343	0,365	0,356

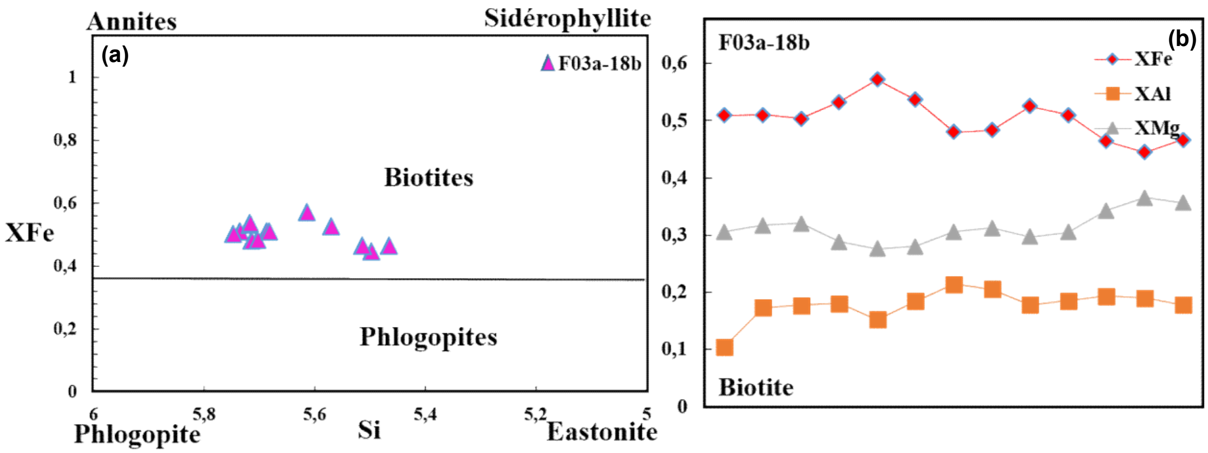

Figure 6. a) biotite nomenclature in the XFe-Si diagram [35]; b) chemical profile of biotite.

Phengite:-The electron microprobe analyses of the micas were projected into crystallochemical diagrams in order to characterize the chemism of the different phases belonging to the mica series. They correspond to secondary muscovites (Figure. 7b) in the diagram of[36]. As for the diagram of [37], and the diagram of Classification of the representative phases of muscovites in the Abilelaï micaschists, they correspond to phengites with Si higher than 6.3 (Figure 7b, c). Phengite and ferriphengite are known to be the usual micas in the epizone of metamorphic series formed at high pressure[38].

Table 3.Representative electron microprobe analyses of phengite. Structural formulas calculated on the basis of 22 oxygen anions. Note phengite in micaschist (analysis 36). C: circle

Rock type	Micaschist									
Sample	AB06a-19									
Analysis	C1a-1	C1a-2	C1a-6	C1a-7	C2a-1	C2a-2	C2b-4	C2b-5	C3a-4	C3a-5
SiO_2	48,7	49,13	47,67	46,03	51,74	48,69	49,99	48,30	48,17	50,15
Al_2O_3	27,61	30,39	30,27	31,48	28,54	30,45	31,86	30,62	30,21	30,41
TiO_2	0,53	0,67	0,58	0,65	0,62	0,67	0,75	0,82	0,53	0,6
FeO	3,14	2,41	2,21	2,22	2,21	2,18	2,19	3,81	2,32	2,32
MnO	0,08	0,1	0,00	0,04	0,00	0,00	0,00	0,01	0,00	0,00
MgO	2,66	1,81	1,94	1,75	2,81	1,95	1,90	1,83	1,93	2,07
CaO	0,00	0,00	0,00	0,00	0,00	0,00	0,00	0,00	0,00	0,00
Na_2O	0,24	0,18	0,24	0,25	0,22	0,32	0,26	0,23	0,26	0,22
K_2O	9,86	9,61	10,52	10,13	10,04	10,32	9,48	9,26	10,57	10,32
Total	**92,83**	**94,29**	**93,42**	**92,56**	**96,18**	**94,59**	**96,43**	**94,89**	**94,00**	**96,08**
Si	6,688	6,586	6,497	6,333	6,794	6,537	6,530	6,478	6,527	6,614
Al^{iv}	1,312	1,414	1,503	1,667	1,206	1,463	1,470	1,522	1,473	1,386
Al^{vi}	3,158	3,389	3,361	3,439	3,212	3,357	3,437	3,320	3,353	3,343
Altotal	4,470	4,803	4,864	5,106	4,418	4,820	4,907	4,842	4,826	4,729
Ti	0,055	0,068	0,059	0,067	0,061	0,068	0,074	0,083	0,054	0,060
Fe^{2+}	0,361	0,270	0,252	0,255	0,243	0,245	0,239	0,427	0,263	0,256
Fe^{3+}	0,000	0,000	0,000	0,000	0,000	0,000	0,000	0,000	0,000	0,000
Mn	0,009	0,011	0,000	0,005	0,000	0,000	0,000	0,001	0,000	0,000
Mg	0,544	0,362	0,394	0,359	0,550	0,390	0,370	0,366	0,390	0,256
Ca	0,000	0,000	0,000	0,000	0,000	0,000	0,000	0,000	0,000	0,000
Na	0,064	0,047	0,063	0,067	0,056	0,083	0,066	0,060	0,068	0,056
K	1,727	1,644	1,829	1,778	1,682	1,768	1,580	1,584	1,827	1,737
Total	**13,918**	**13,790**	**13,958**	**13,969**	**13,804**	**13,911**	**13,766**	**13,841**	**13,954**	**13,858**
Mg#	0,601	0,573	0,610	0,585	0,694	0,614	0,608	0,462	0,597	0,500

XFe	0,163	0,132	0,117	0,112	0,122	0,117	0,115	0,184	0,124	0,135
XMg	0,245	0,177	0,183	0,157	0,275	0,186	0,178	0,158	0,183	0,135
XAl	0,592	0,691	0,699	0,731	0,603	0,697	0,707	0,657	0,693	0,730

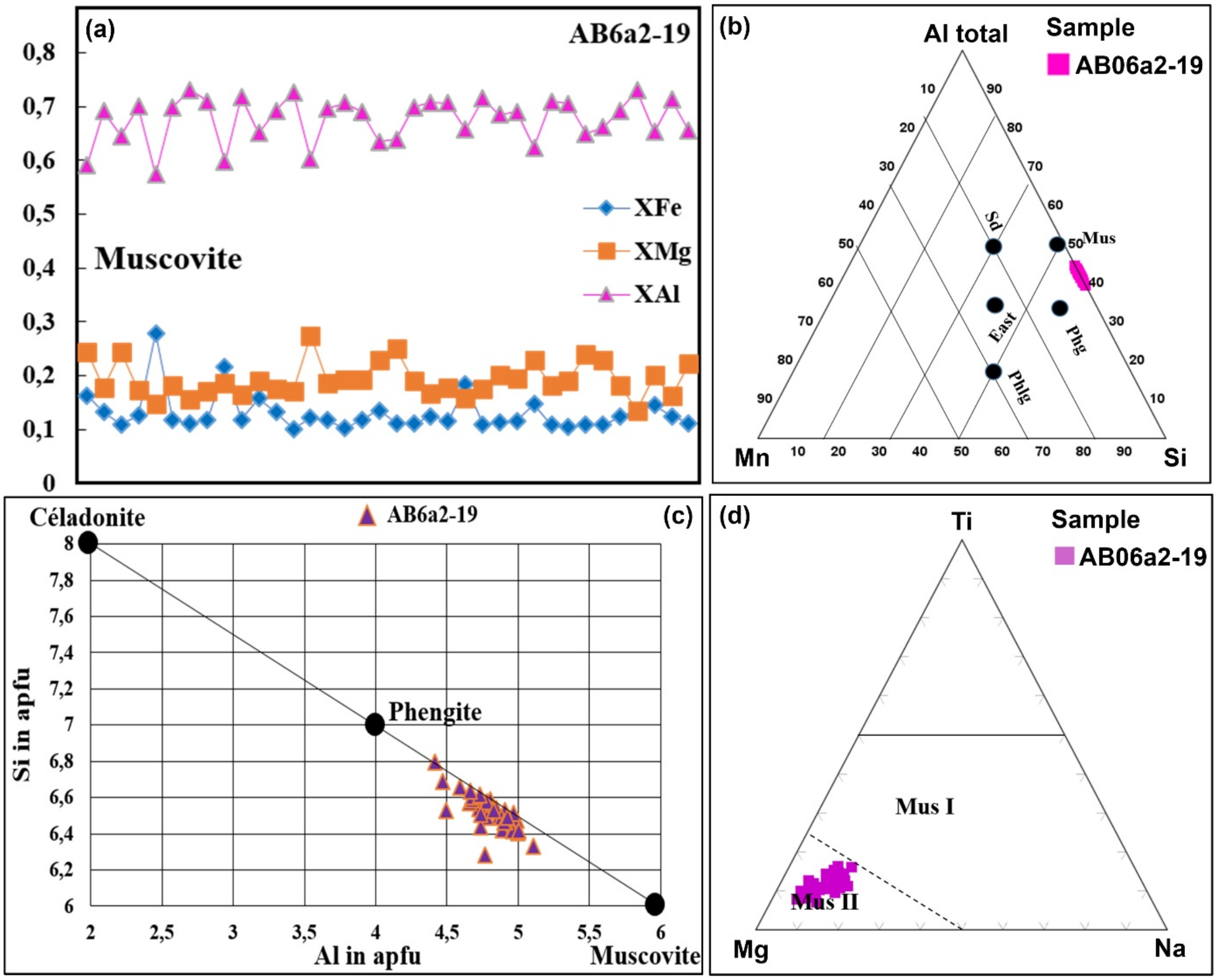

Figure7. a) Chemical profile of muscovite.b) Classification of micas of[37].c) Classification of representative phases of muscovites in Abilelaï micaschists [32].b) Position of muscovites from micaschists in the diagram of [36].

Feldspar:-

Feldspar in garnet micaschists (sample F03a-18b) of the South massif Ouaddaï areas typically has a plagioclase (albite) composition (Table 4). The orthoclase component varies between 0.38 and 0.85%. However, these plagioclases don't show significantvariation ($CaAl_2Si_2O_8$-$NaAlSi_3O_8$). In garnet micaschist, plagioclase cristals yield K-poor albite ($An_{4.36-6.86}Ab_{92.43-94.79}Or_{0.38-0.85}$) compositions.

Table 4.Representative electron microprobe analyses of feldspar. Structural formulas calculated on the basis of 8 oxygen anions. Note plagioclase in micaschist of garnet (analysis 11) and calc-silicate gneisses (analysis 15). C: circle

Rock type	Garnet-Micaschists					Calc-silicate gneisses				
Sample	F03a-18b					F06b-18				
Analysis	C2c-1	C2c-2	C2c-3	C3b-1	C3b-2	C1b-1	C1b-2	C3b-1	C3b-2	C3b-3
SiO_2	65,75	65,66	65,8	65,79	66,01	58,3	57,98	57,67	57,59	57,16
Al_2O_3	20,68	20,69	21,10	20,34	20,18	25,77	25,41	25,82	26,11	26,3

TiO_2	0,01	0,00	0,00	0,00	0,00	0,00	0,01	0,02	0,00	0,00
FeO	0,12	0,00	0,00	0,12	0,04	0,00	0,03	0,10	0,12	0,05
MnO	0,00	0,00	0,08	0,00	0,00	0,00	0,00	0,00	0,01	0,04
MgO	0003	0,01	0,02	0,00	0,00	0,04	0,01	0,00	0,00	0,01
CaO	1,52	1,51	1,48	1,44	1,08	8,11	7,78	8,40	8,26	8,47
Na_2O	11,72	11,32	11,65	11,49	11,7	7,43	7,37	7,29	7,20	7,31
K_2O	0,09	0,09	0,08	0,1	0,13	0,20	0,17	0,16	0,21	0,20
Total	**99,92**	**99,28**	**100,21**	**99,28**	**99,14**	**99,85**	**98,76**	**99,46**	**99,50**	**99,57**
Si	2,902	2,909	2,893	2,918	2,929	2,617	2,627	2,602	2,597	2,580
Altotal	1,076	1,081	1,094	1,063	1,055	1,364	1,358	1,374	1,388	1,400
Ti	0,000	0,000	0,000	0,000	0,000	0,000	0,000	0,001	0,000	0,000
Fe^{2+}	0,004	0,000	0,000	0,004	0,001	0,000	0,001	0,004	0,005	0,002
Fe^{3+}	0,000	0,000	0,000	0,000	0,000	0,000	0,000	0,000	0,000	0,000
Mn	0,000	0,000	0,003	0,000	0,000	0,000	0,000	0,000	0,000	0,002
Mg	0,002	0,001	0,001	0,000	0,000	0,003	0,001	0,000	0,000	0,001
Ca	0,072	0,072	0,070	0,068	0,051	0,390	0,378	0,406	0,399	0,410
Na	1,003	0,972	0,993	0,988	1,006	0,647	0,648	0,638	0,629	0,642
K	0,005	0,005	0,004	0,006	0,007	0,011	0,010	0,009	0,012	0,012
Total	**5,064**	**5,039**	**5,059**	**5,048**	**5,051**	**5,031**	**5,022**	**5,034**	**5,030**	**5,047**
An	6,67	6,86	6,55	6,40	4,79	37,21	36,49	38,56	38,37	38,53
Ab	92,87	92,66	92,89	93,03	94,55	61,74	62,55	60,59	60,48	60,34
Or	0,46	0,48	0,56	0,56	0,66	1,05	0,97	0,85	1,15	1,13

Garnet:-

The data obtained from the electron microprobe and Structural formulas calculated shows that the garnet is of almandine typeand amount varying between 75 and 85% (Table. 5; Figure 8a, c). Similarly, the chemical profile of the garnet shows an enrichment in FeO (Figure. 8b, d,). As for the chemical variation of the garnet, it is not so important between the edge and the core (Figure. 8c).

Sample F06b-18 shows the proportion of grossular and almandine is close (Figure 8e). Thus, the calc silicate gneisses shows a slightly higher calcium content than the garnet found in micaschists. The chemical variation between rim and core is not significant (Figure 8f).

Table 5.Representative electron microprobe analyses of garnet. Structural formulas calculated on the basis of 12 oxygen anions. Note garnet-micaschist (analysis 11), staurolite-micaschist (analysis 15) and calc-silicate gneisses (analysis 12). C: circle; b: border; c: core.

Rock type Garnet- Micachists Staurolite- Micashist Calc-silicate gneisses																				
Sample F03a-18b F04a-18 F06b-18																				
Analysis	C3a-1b	C3a-2b	C3a-3b	C3a-4c	C3a-5c	C1c-1b	C1c-2b	C1c-3c	C1c-4c	C1d-1b	C4a-1b	C4a-2b	C4a-3c	C4a-4c	C5a-1b	C5a-2b	C5a-3c	C5a-4c	C6a-1b	C6a-2b
SiO_2	36,33	36,34	36,04	36,29	35,77	36,67	36,52	36,74	36,71	36,23	37,53	37,04	37,69	37,14	37,03	36,87	37,19	37,20	37,43	36,95
Al_2O_3	21,28	20,86	20,75	20,62	20,74	21,01	21,3	20,87	20,93	20,81	20,89	20,89	20,88	20,86	20,98	20,96	20,65	20,83	20,63	20,57
TiO_2	0,00	0,00	0,02	0,00	0,00	0,03	0,00	0,05	0,01	0,01	0,07	0,05	0,08	0,04	0,02	0,02	0,04	0,04	0,05	0,04
FeO	36,28	35,8	34,5	36,1	36,5	37,98	37,0	36,1	36,7	37,8	21,1	21,21	19,89	19,0	20,2	20,5	20,4	21,8	19,3	19,0

		0	2	2	9		9	2	4	8	4			3	0	5	9	2	5	8
MnO	3,79	3,77	5,33	3,47	2,87	0,4	0,79	1,11	1,28	0,53	2,92	3,26	3,45	3,84	3,11	4,19	3,26	3,63	2,05	2,81
MgO	2,28	2,22	1,82	2,34	2,29	2,82	2,88	2,29	2,44	2,64	0,82	0,73	0,63	0,64	0,74	0,85	0,68	0,73	0,77	0,73
CaO	0,67	0,84	0,99	0,94	0,74	1,15	1,10	1,74	1,70	1,14	16,35	17,29	17,42	17,23	16,95	15,72	17,01	15,44	18,63	16,91
Na_2O	0,00	0,00	0,16	0,00	0,00	0,28	0,09	0,02	0,03	0,02	0,00	0,00	0,07	0,00	0,00	0,00	0,06	0,03	0,01	0,00
K_2O	0,00	0,00	0,02	0,00	0,00	0,01	0,00	0,00	0,00	0,00	0,01	0,01	0,01	0,03	0,00	0,00	0,02	0,01	0,02	0,00
Total	**100,63**	**99,83**	**99,66**	**99,79**	**99,00**	**100,36**	**99,77**	**98,94**	**99,86**	**99,27**	**99,74**	**100,48**	**100,13**	**98,82**	**99,02**	**99,15**	**99,41**	**99,72**	**98,96**	**97,08**
Si	2,946	2,968	2,960	2,969	2,951	2,966	2,962	3,001	2,982	2,966	2,982	2,939	2,982	2,975	2,963	2,956	2,972	2,970	2,985	2,998
Altotal	2,035	2,009	2,009	1,989	2,017	2,004	2,037	2,010	2,004	2,008	1,957	1,954	1,948	1,970	1,979	1,981	1,954	1,961	1,940	1,968
Ti	0,000	0,000	0,001	0,000	0,000	0,002	0,000	0,003	0,001	0,001	0,004	0,003	0,005	0,002	0,001	0,001	0,002	0,002	0,003	0,002
Fe^{2+}	2,461	2,446	2,371	2,471	2,525	2,569	2,516	2,468	2,496	2,594	1,405	1,408	1,316	1,275	1,352	1,378	1,369	1,457	1,291	1,295
Fe^{3+}	0,000	0,000	0,000	0,000	0,000	0,000	0,000	0,000	0,000	0,000	0,000	0,000	0,000	0,000	0,000	0,000	0,000	0,000	0,000	0,000
Mn	0,260	0,261	0,371	0,240	0,201	0,027	0,054	0,077	0,088	0,037	0,197	0,219	0,231	0,261	0,211	0,285	0,221	0,246	0,138	0,193
Mg	0,276	0,270	0,223	0,285	0,282	0,340	0,348	0,279	0,295	0,322	0,097	0,086	0,074	0,076	0,088	0,102	0,081	0,087	0,092	0,088
Ca	0,058	0,074	0,087	0,082	0,065	0,100	0,096	0,152	0,148	0,100	1,392	1,470	1,477	1,479	1,453	1,350	1,456	1,321	1,592	1,470
Na	0,000	0,000	0,025	0,000	0,000	0,044	0,014	0,003	0,005	0,003	0,000	0,000	0,011	0,000	0,000	0,000	0,009	0,005	0,002	0,000
K	0,000	0,000	0,002	0,000	0,000	0,001	0,000	0,000	0,000	0,000	0,001	0,001	0,001	0,003	0,000	0,000	0,002	0,001	0,002	0,000
Total	**8,036**	**8,027**	**8,049**	**8,037**	**8,040**	**8,053**	**8,027**	**7,993**	**8,018**	**8,031**	**8,035**	**8,081**	**8,045**	**8,040**	**8,047**	**8,052**	**8,059**	**8,050**	**8,044**	**8,015**
Py	9,03	8,85	7,31	9,26	9,18	11,20	11,55	9,38	9,75	10,55	3,14	2,70	2,39	2,46	2,84	3,27	2,59	2,80	2,96	2,89
Alm	80,56	80,17	77,69	80,28	82,17	84,62	83,48	82,93	82,46	84,97	45,45	44,23	42,48	41,25	43,56	44,24	43,78	46,83	41,47	42,51

Spes	8,51	8,55	12,16	7,80	6,54	0,89	1,79	2,59	2,91	1,21	6,37	6,88	7,46	8,44	6,80	9,15	7,07	7,91	4,43	6,34
Gros	1,90	2,43	2,85	2,66	2,12	3,29	3,19	5,11	4,89	3,28	45,03	46,18	47,68	47,85	46,81	43,34	46,56	42,46	51,14	48,26

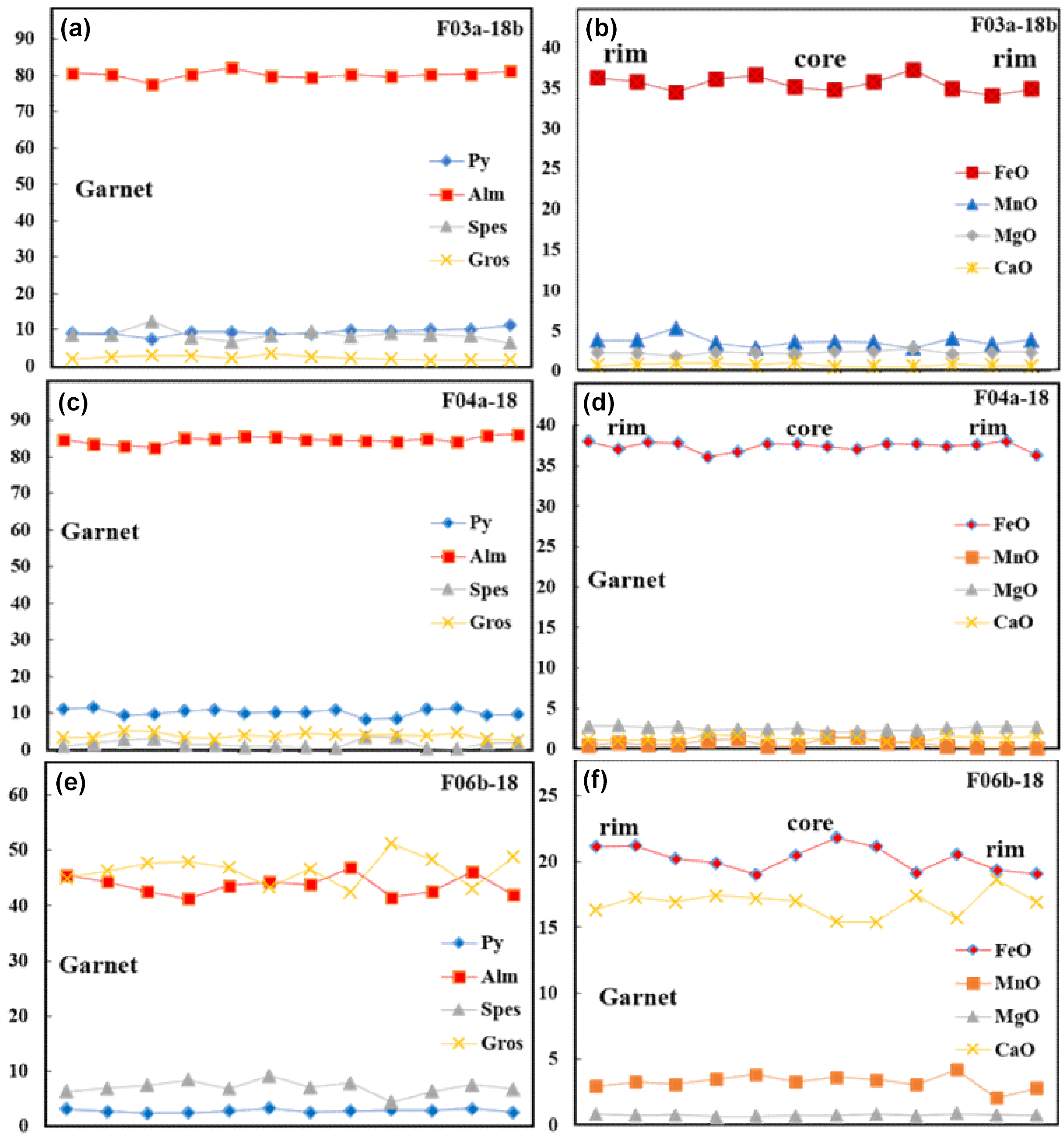

Figure8. (a), (c) Chemical profile showing almandine garnet (b), (d) Chemical profile showing iron-rich garnet and there is not enough chemical variation at the rim and the core (e) chemical profile showing grossular and almandine garnet (f) chemical variation at the rim and the core of garnet.

Amphibole:-

The arrangement of amphiboles in the South Ouaddaï region in the nomenclature diagram (Figure 9a) of [39]shows an evolution of actinote, magnesio-hornblende and Tschermakite (metamorphic amphibole). Amphibole minerals such as Tschermakite are hydrated (contain an OH group), they can decompose into denser anhydrous minerals such as pyroxene or garnet at high temperatures [40].

Representative microprobe analyses are listed in Table 7. Structural formulas were calculated on the basis 13 anions except Ca, Na, K cations, i.e. Si + Ti +Al + Fe + Mg +Mn = 13,00 a.p.f.u and 23 oxygen anions. A total of nine compositions yield totals of ~97.21 wt% (Table 6).

Table 6.Representative electron microprobe analyses of amphiboles. Structural formulas calculated on the basis of 23 oxygen anions. Note garnet in calc-silicate gneisses (analysis 12). C : circle

Rock type	Calc- silicate gneisses								
Sample	F06b-18								
Analysis	**C1-1**	**C1-2**	**C1-3**	**C1-4**	**C1-5**	**C1-6**	**C1-7**	**C1-8**	**C1-9**
SiO2	49,72	40,91	41,22	41,09	40,46	51,22	44,85	40,28	39,50
Al2O3	2,47	12,2	11,73	12,11	12,42	2,58	9,66	13,26	13,44
TiO2	0,01	0,44	0,44	0,34	0,45	0,05	0,04	0,57	0,59
Fe_2O_3	0	0	0	0	0	0	0	0	0
FeO	23,85	22,21	22,16	22,73	22,41	19,08	20,13	21,06	20,53
MnO	0,35	0,52	0,51	0,41	0,41	0,44	0,62	0,33	0,50
MgO	9,07	6,22	6,21	6,97	5,99	10,95	8,36	6,46	6,19
CaO	12,21	12,19	11,88	10,9	12,35	12,63	12,32	11,95	11,71
Na2O K2O	0,09 0,13	1,23 1,71	1,06 1,64	0,90 1,30	0,98 1,71	0,23 0,19	0,96 0,86	2,02 1,93	1,04 2,05
Total	**97,90**	**97,63**	**96,85**	**96,75**	**97,18**	**97,37**	**97,80**	**97,86**	**95,55**
Si	7,471	6,044	6,154	6,136	6,023	7,594	6,580	6,244	6,251
Al^{IV}	0,529	1,956	1,846	1,864	1,977	0,406	1,420	1,750	1,749
Al^{VI}	0,000	0,168	0,218	0,268	0,202	0,045	0,250	0,673	0,758
Ti	0,001	0,049	0,049	0,038	0,050	0,006	0,004	0,066	0,070
Fe^{3+}	0,669	2,365	2,149	2,028	2,282	0,452	1,595	2,437	2,306
Fe^{2+}	2,328	0,379	0,618	0,811	0,508	1,914	0,875	0,293	0,275
Mn	0,045	0,065	0,064	0,052	0,052	0,055	0,077	0,043	0,067
Mg	2,031	1,369	1,382	1,551	1,329	2,420	1,828	1,492	1,460
Ca	1,966	1,930	1,900	1,744	1,970	2,007	1,937	1,985	1,986
Na	0,026	0,070	0,100	0,256	0,030	0,000	0,063	0,136	0,114
K	0,025	0,322	0,312	0,248	0,325	0,036	0,161	0,358	0,393
Na_A	0,000	0,282	0,207	0,005	0,253	0,073	0,210	0,434	0,189
A	0,025	0,604	0,520	0,252	0,577	0,109	0,371	0,793	0,582

Clinopyroxene:-

The classification of pyroxene in the diagram of [41]shows an intermediate composition between diopside and hedenbergite (Figure 9b). The latter are particularly typical of calcium-rich sediments that have undergone metamorphism. Diopside occurs early in a prograde metamorphic sequence of silica- and dolomite-bearing sediments. Clinopyroxenes with an intermediate diopside-hedenbergite composition occur in calcium-rich sedimentary zones[32]. Electron microprobe data allowed the calculation of 6-oxygen structural formulae.

Table 7. Representative electron microprobe analyses of clinopyroxene. Structural formulas calculated on the basis of 06 oxygen anions. Note garnet in calc-silicate gneisses (analysis 13). C: cercle.

Rock type	Calc-silicate gneisses									
Sample	F06b-18									
Analysis	C1c-1	C1c-2	C1d-1	C1d-2	C1e-1	C1e-2	C1e-3	C1e-4	C1e-5	C2b-1
SiO_2	50,50	50,86	50,22	50,42	50,58	50,29	50,35	50,64	50,07	50,53
Al_2O_3	0,90	1,07	0,46	0,99	0,21	1,02	0,46	0,81	0,83	0,75
TiO_2	0,01	0,02	0,02	0,00	0,00	0,04	0,04	0,04	0,00	0,04
FeO	15,92	14,02	17,12	15,03	15,15	15,54	14,98	14,93	16,12	15,03
MnO	0,22	0,34	0,71	0,29	0,65	0,27	0,42	0,26	0,50	0,43
MgO	8,41	9,26	7,54	8,59	8,60	8,34	8,76	9,20	8,38	8,6
CaO	23,55	22,79	23,61	23,26	23,74	23,17	23,31	23,81	23,3	23,87
Na_2O	0,34	0,33	0,17	0,38	0,13	0,23	0,12	0,36	0,27	0,25
K_2O	0,04	0,06	0,00	0,02	0,02	0,05	0,06	0,01	0,01	0,01
Total	**99,99**	**98,93**	**99,84**	**98,98**	**99,08**	**98,95**	**98,51**	**100,08**	**99,47**	**99,50**
Si	1,965	1,979	1,971	1,971	1,982	1,970	1,979	1,960	1,961	1,968
Al^{iv}	0,035	0,021	0,021	0,029	0,010	0,030	0,021	0,037	0,038	0,032
Al^{vi}	0,006	0,028	0,000	0,017	0,000	0,017	0,000	0,000	0,000	0,002
Altotal	0,041	0,049	0,021	0,046	0,010	0,047	0,021	0,037	0,038	0,034
Ti	0,000	0,001	0,001	0,000	0,000	0,001	0,001	0,001	0,000	0,001
Fe^{2+}	0,518	0,456	0,562	0,491	0,496	0,509	0,492	0,483	0,528	0,490
Fe^{3+}	0,000	0,000	0,000	0,000	0,000	0,000	0,000	0,000	0,000	0,000
Mn	0,007	0,011	0,024	0,010	0,022	0,009	0,014	0,009	0,017	0,014
Mg	0,488	0,537	0,441	0,500	0,502	0,487	0,513	0,531	0,489	0,499
Ca	0,982	0,950	0,993	0,974	0,997	0,972	0,982	0,987	0,978	0,996
Na	0,026	0,025	0,013	0,029	0,010	0,017	0,009	0,027	0,020	0,019
K	0,002	0,003	0,000	0,001	0,001	0,002	0,003	0,000	0,000	0,000
Total	**4,028**	**4,010**	**4,025**	**4,021**	**4,019**	**4,015**	**4,015**	**4,035**	**4,031**	**4,023**

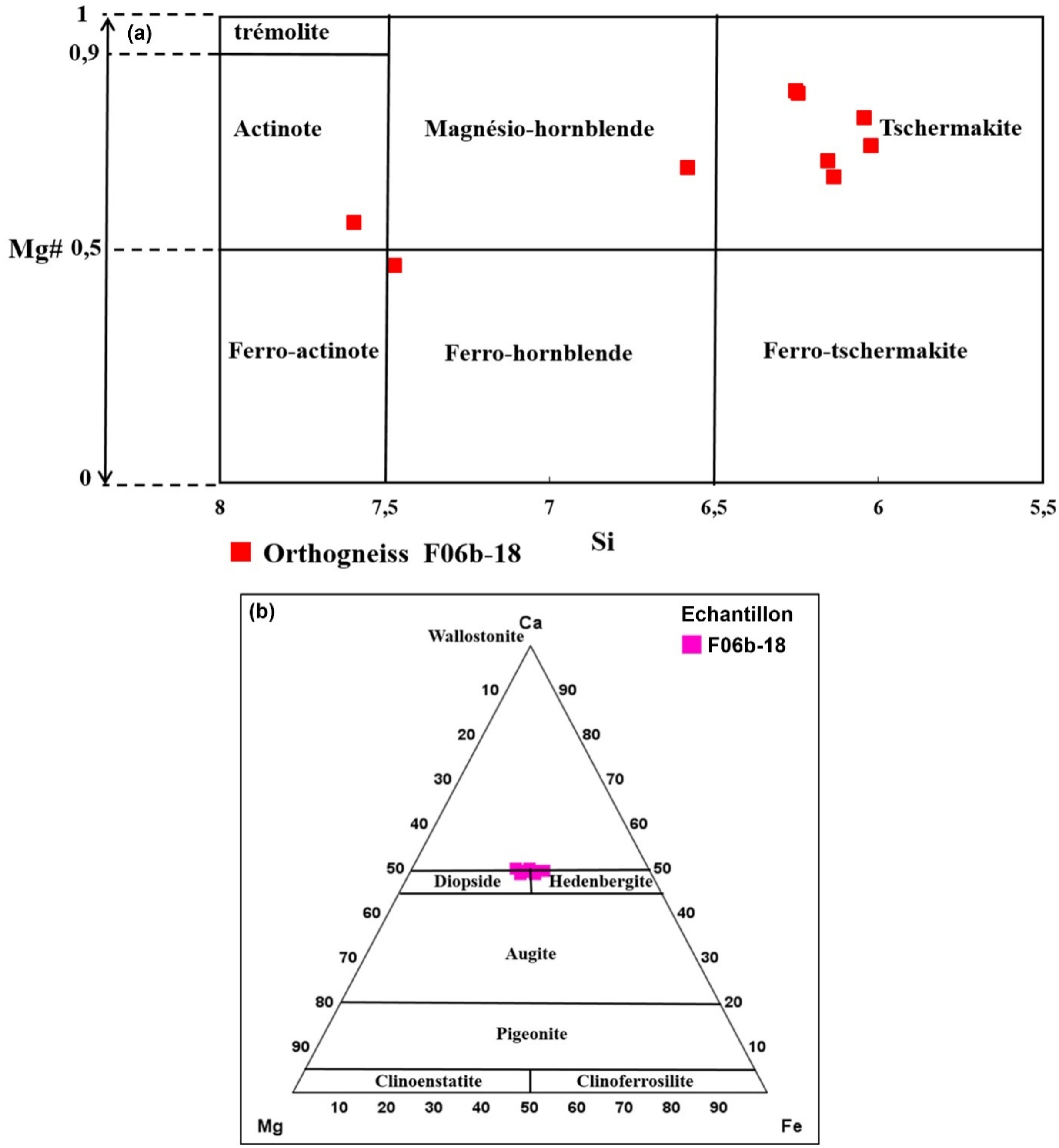

Figure9.(a) Amphibole classification diagram after [39],showing the actinolite, magnesio-horblende and tschermakite compositions of the measured amphiboles in sample F06b-18. (b)Position of pyroxenes in the Ca-Fe-Mg diagram of [41].

Discussion:-

In this section, we discuss the results obtained in the previous sections. The structural record of the study area is defined by three distinct phases characterized by a regional flat lying foliation (D1) overprinted by steep sinistral S2 shear zones (D2) under transpressive tectonic conditions, resulting in S0/S1 planes being folded by F2 folds admitting an axial plane S2. Both dip direction and strike of S1 surfaces where significantly shifted by S2 suggesting that during the second phase, F2 folds formed with inclined axes. This is clear from field observations. Further, evidence of transpression is attested by D2 folding of S1 foliation and the presence of gently plunging L2 lineation indicating a shearing component. D1 and D2 structures are cut by late discrete dextral shear zones. These observations suggest a dominant movement following a NW-SE direction.

Pressure shadows:-

In sample F04a-18, the most common type of pressure shadow is the σ shadow, which forms from a rigid body that has undergone relatively little or no rotation. In this case, the tip of the shadow points in the direction of motion (Fig. 4k). The tails generally consist of an aggregate of polycrystalline materials of a similar nature (quartz crystals).

Analysis of the relationship between garnet generation, the pressure shadow, and the orientations of the mica minerals (Ms + Bt) in Figure 5 above reveals the presence of two generations of micas, associated with two distinct deformation episodes (D1-D2). First, there are oblique micas associated with S1 schistosity, and second, horizontal micas associated with S2 schistosity. The syn-tectonic nature of the garnets identified in these sections links them to this second deformation phase D2 (Figure. 4l).

Low-grade rocks:-

The low-grade rocks are described in the NW of the study area where the metamorphic assemblages are characterized by chlorite + sericite + actinote + epidote + vapor as excess phases. Samples AB15-19 is a chloritoschist.Under the microscope, it is well observed that the schistosity S1 is folded. The mineralassociation underlining S1made up of sericite + chlorite+ quartz is typical of the chloritoschit zone.Accordingly, this part of the study area belongs to a greenschist facies.The texture of quartz grains allowed the identification of detrital minerals and neoformed minerals. Large grains (Qtz1) with rolling extinction and recrystallized medium-sized grains (Qtz2) in the foliation may correspond to detrital quartz (Figure4i). Neoformed quartz usually developed as crystals exhibiting well-defined shapes (Figure4i). According to their internal microstructures, the recrystallized quartz grains probably formed at the temperature interval between 300 and 400°C [30].

Medium to high-grade rocks:-

Medium to high-grade rocks occur in the southeastern part of the study area. Some samples belonging to this metamorphic grade are described below.Sample F03a-18b described from this part shows a lepidogranoblastic texture. It is grey to brown and the mineralogical assemblage is made of the following minerals: quartz, muscovite, biotite, garnet and plagioclase. Garnet is an idiomorphic porphyroblast of variable size (2 to 5 mm), often cracked includingquartz and mica. It is also observed as a corona along pyroxene crystals (Garnet Zone). Sillimanite crystals in equilibrium with garnet are replaced by an assemblage including muscovite. Rare kyanite minerals may be observed and they correspond to an assemblage typifying higher metamorphic grade than the sillimanite zone. Following thisdescription the successive metamorphic assemblages, corresponding to a retrograde path is inferred: pyroxene + kyanite (granulite) = > garnet + sillimanite + biotite (amphibolite) = > muscovite + biotite + albite +/- chlorite (greenschist). Along the S2 planes, it appears from microscopic observations that almandine garnet porphyroblats (Fig. 5l), corresponding to the upper amphibolite facies (Bt + Gt) is overprinted by a greenschist facies assemblage (quartz + muscovite + biotite + albite). Accordingly, the second deformation phase occur under retrograde metamorphic conditions.

Staurolite is a characteristic mineral of the middle metamorphic grade of metapelites, which is why [32],point out that the mineral belongs to the "regional metamorphic zone".Hence, sample (F04a-18) corresponds to the medium-grade metamorphic assemblage observed in the study area to the SE. Staurolite crystals are generally rich in iron, with XMg (Mg / Mg + Fe)< 0.3. The metamorphic condition indicates that their formation is within the experimentally determined stability domain of Fe-staurotide + quartz, i.e. P > 0.15GPa and T = 500-700°C [32].[42]correlated the composition of staurolite with the metamorphic grade of the Barrovian sequence of biotite, garnet and staurolite-kyanite zones in the enclosing pelitic schists.

The metamorphic imprint shows contrasting conditions in the NW and SE parts of the study area. Actually, while greenschist-amphibolite facies dominates in the NW, the SE is characterized by higher grades with the presence of relictual granulitic mineral assemblages. In both parts, the early higher grade metamorphic condition is retrogressed to greenschist facies assemblages indicated by late overgrowth of minerals such as chlorite, epidote and calcite. Accordingly, D1 is assumed to accommodate a gradual exhumation of the lower parts of the continental crust from the NW to the SE. The preservation of high-grade relictual assemblages probably reflect the lack of fluid expelled during the prograde evolution. The succession of a prograde and retrograde metamorphic evolution, also depicted as a clockwise evolution, denote an evolution from burial to exhumation of continental rocks in collision zones [43].

Finally, the Southern Ouaddaï Massif displays petrological and tectonic features significantly distinct from the adjacent Guera [21]and Mayo Kebbi Massifs [44], interpreted as juvenile Neoproterozoic crustal domains. Both its isotopic [17]and metamorphic evolution suggest a complex history indicating remobilisation through erosion, sedimentation, burial, melting and exhumation of pre-Neoproterozoic materials in a tectonic setting where only a small part of mantle contribution occurred during the Pan-African times. Such a context may relate to passive margin environment, where detrital materials associated to carbonate precipitation, were synchronous to mafic dykes intrusions during the rifting episode of the Wilson Cycle. This rifted crust was subsequently involved into continental collision and metamorphism, as well as heating and partial melting of the metasedimentary rocks after crustal thickening.

This evolution is generally similar to that of the southern part of the CAOB [45, 46, 47].It differs from the central part in that metasedimentary rocks predominate over syn-tectonic calc-alkaline orthogneisses [48, 5,9, 19, 49], whereas the northern domain is primarily of a younger nature. According to[17], U-Pb isotopic data on zircon show that the metasedimentary rocks of the southern Ouaddaï massif indicate ages ranging from the Archean to the Paleoproterozoic (approximately 3.0 Ga and approximately 1.9 Ga), interpreted as the age of the protoliths of these metamorphic rocks. These sedimentation ages are similar to those of the Lower Tibestian (approximately 1–0.8 Ga) identified in northern Chad [50, 51].

A concordant U-Pb age of 602 ± 3 Ma defines the age of the syn-tectonic leucogranites and corresponds to the second deformation phase, D2. However, as suggested by[3], D1 likely occurred around 620 Ma and marks a regional collision event also described in Cameroon [3]and Central Africa [52]. The NW-SE direction is perpendicular to the directions of these three deformation phases (D1, D2, and D3) and corresponds to the dip of lineations L1 and L2. These directions agree with those of the quartz veins containing gold mineralization described [53, 54].

Conclusion:-

The microstructural analyses of the southern part of the Ouaddaï massif show three deformation phaseshave been identified.D1is observed within the metasedimentary rock units and corresponds to a composite S0/S1-type foliation.D2 is marked by S2 schistosity, characterised by a preferential orientation of the feldspar minerals and the flake-like arrangement of the micas.D3 is associated with several families of brittle deformation, characterized by dry joints and joints filled by magmatic material in the form of aplitic and pegmatitic veins trending predominantly NE-SW.The metamorphic imprint shows contrasting conditions in the NW and SE parts of the study area. Actually, while greenschist-amphibolite facies dominates in the NW, the SE is characterized by higher grades with the presence of relictual granulitic mineral assemblages. In both parts, the early higher-grade metamorphic condition is retrogressed to greenschist facies assemblages indicated by late overgrowth of minerals such as chlorite, epidote and calcite. These mineralogical analyses make it possible to characterise the chemistry of the mineral phases of the metasediments.

Acknowledgement:-

This paper is issued from part of Malik Hisseine Malik Ph.D. thesis, for which he benefited from scholarschip at the Agency of Francophony University (AUF). This thesis is an integral part of the AUF project N° DRACGL-2017-005 within the framework of a vast program entitled "Geodynamic controls of gold, uranium and rare metal concentrations during the Pan-African orogeny: Example of the Central African Orogenic Belt (Chad, Cameroon and Central African Republic)" driven by Dr Moussa ISSEINI and the research programmes developed by Pr Anne-Sylvie ANDRE-MAYER in the African Proterozoic belts.

Bibliographic References:-

1. Abdelsalam, M.G., Liegeois, J.P., Stern, R.J., 2002.The Saharan metacraton. Journal of African Earth Sciences, 34, 119-136.
2. Abdelsalam, M.G., El-Shaikh, M.A., El-Fadil, M., Bushra, A., Fathel-Rahman, M.E., Stern, R.J., Allison, K.T., 2003.Neoproterozoic deformation in the northeastern part of the Saharan Metacraton, northernSudan. Precambrian Research, 123, P 203–221.
3. Toteu, S.F., Penaye, J., Poudjom Djomani, Y., 2004. Geodynamic evolution of the Pan-African belt in central Africa with special reference to Cameroon. Canadian Journal of Earth Sciences 41, 73–85.
4. Penaye, J., Kröner, A., Toteu, S.F., Van Schmus, W.R., Doumnang, J.C., 2006. Evolution of the Mayo Kebbi region as revealed by zircon dating: An early (ca. 740Ma) Pan-African magmatic arc in southwestern Chad. Journal of African Earth Sciences 44: 530–542.
5. Ngako V., Affaton P., Njonfang E., 2008.Pan-African tectonics in northwestern Cameroon: Implication for the history of western Gondwana. Gondwana Research, 14, P 509–522.
6. Ngako, V., Njonfang, E., 2011. Plates amalgamation and plate destruction, the Western Gondwana history. In: D. Closson (Ed.), Tectonics. INTECH, UK, 3-34 p.

7. Feybesse, J.L., Johan, V., Triboulet, C., Guerrot, C., Mayaga-Mikolo, F., Bouchot, V., Eko N'Dong, J., 1998. The west Central Africa belts: a model of 2.5-2.0 Ga accretion and two-phase orogenic evolution. Precambrian Research 87: 161-216.
8. Toteu, S.F., Van Schmus, R.W., Penaye, J., Michard, A., 2001. New U– Pb and Sm–Nd data from north-central Cameroon and its bearing on the pre-Pan-African history of central Africa. Precambrian Research 108, 45–73.
9. Affaton, P., 2011. Pan-African metamorphic evolution in the southern part of the Yaoundé Group (Oubanguide Complex, Cameroon), as revealed by EMP dating of monazite and thermobarometry of garnet metapelites. J. Afr. Earth Sci. 59, 125–139.
10. Oliveira, E.P., Toteu, S.F., Araujo, M.N.C., Carvalho, M.J., Nascimento, R.S., Bueno, J.F., Mc Naughton, N., Basilici, G., 2006. Geologic correlationbetween the Neoproterozoic Sergipano belt (NE Brazil) and the Yaoundé Belt (Cameroon,Africa). Journal of African Earth Sciences 44: 470-478.
11. Theunissen, K., Lenoir, J.L., Liegeois, J.P., Delvaux, D., Murma, A., 1992. Major Pan-African imprint in the Ubendian range of southwestern Tanzania: U-Pb geochronology on zircon and structural context. C.R. Académie des Sciences Paris 314: 1355–1362.
12. Bessoles, B., Trompette, R., 1980. Geology of Africa. The Pan-African Belt: “Central African Mobile Zone (southern part) and Sudanese Mobile Zone.” B.R.G.M. Memoir, Orléans, 92: 394.
13. Castaing, C., Feybesse, J.L., Thieblemont, D., Triboulet, C., Chevrement, P., 1994. Paleogeographical reconstructions of the Pan-African/Brasiliano orogen: closure of an oceanic domain or intracontinental convergencebetween major blocks? Precambrian Research 69: 327-344.
14. Liégeois, J.P., Latouche, L., Boughara, M., Navez, J., Guiraud, M., 2003.The LATEA metacraton, (central Hoggar, Tuareg shield, Algeria): behaviour of an oldpassive margin during the Pan-African orogeny. Journal of African Earth Sciences 37: 161-190.
15. Pouclet, A., Vidal, M., Doumnang, J.C., Vicat, J.-P., Tchameni, R., 2006.Neoproterozoic evolution in the Southern Chad: Pan-African ocean basin closing, arcaccretion and late- to post-orogenic granitic intrusion. Journal of African Earth Sciences 44:543-560.
16. Stendal, H., Toteu, S.F., Frei, R., Penaye, J., Njel, U.O., Jean Nni, J.B., Kankeu, B., Ngako, V., Hell, J.V., 2006.Derivation of detrital rutile in the Yaounde´ region from the Neoproterozoic Pan-African belt in southern Cameroon (Central Africa). Journal of African Earth Sciences 44, 443-468
17. Djerossem, N.F., 2018. Crustal growth and remobilization in the Pan-African in the southern Ouaddaï massif (eastern Chad). Doctoral Thesis in Geosciences at the University of Toulouse, 302 p.
18. Djerossem, N.F., Berger, J., Vanderhaeghe, O., Isseini, M., Ganne, J., Zeh, A., 2020. Neoproterozoic magmatic evolution of the southern part of the Ouaddaï Massif (Chad). Bulletin of the Geological Society of France (BSGF) 191, 34.
19. Bouyo Houketchang, M., Penaye, J., Barbey, P., Toteu, S.F., Wandji, P., 2013. Petrology of high-pressure granulitic facies metapelites and metabasites from the Tcholliré and Banyo regions: geodynamic implications for the Central African Fold Belt (CAFB) in north-central Cameroon. Precambrian Res. 224, 412–433.
20. Liégeois, J.P., Abdelsalam, M.G., Nasser, E., Ouabadi, A., 2013. Metacraton: Nature, genesis and behavior. Gondwana Research, 23, 320-237.
21. Shellnutt, J.G., Pham, N.H.T., Denyszyn, S.W., Yeh, M.-W., Lee, T.-Y., 2017. Timing postcollisional Pan-African Orogeny granitic magmatism within south-central Chad. Precambrian Research 301, 113–123.
22. Shellnutt, J.G., Yeh, M.W., Lee, T.Y., Iizuka Y, Pham NHT, Yang CC. 2018. The origin of Late Ediacaran post-collisional granites near the Chad Lineament, Saharan Metacraton, South-Central Chad. Lithos 304-307: 450–467.
23. Djerossem, F., Zeh, A., Isseini, M., Vanderhaeghe, O., Berger, J., Ganne, J., 2021. U-Pb-Hf isotopic systematics of zircons from granites and metasediments of southern Ouaddaï (Chad), implications for crustal evolution and provenance in the Central Africa Orogenic Belt. Precambrian Research 361 – 106233.
24. Abdelsalam, M.G., Gao, S.S., Liégeois, J.P., 2011. Upper mantle structure of the Saharan metacraton. Journal of African Earth Sciences, 60, P 328-336.
25. Meert, J.G., Lieberman, B.S., 2007. The Neoproterozoic assembly of Gondwana and its relationship to the Ediacaran-Cambrian radiation. Gondwana Research. doi:10.1016/j.gr.2007.06.007.
26. Küster, D., Liégeois, J.P., 2001. Sr, Nd isotopes and geochemistry of the Bayuda Desert high-grade metamorphic basement (Sudan): an early Pan-African oceanic convergent margin, not the edge of the East Saharan ghost craton? Precambrian Res. 109, 1–23.
27. Gsell, J., Sonnet, J., 1960. 1:500,000-scale reconnaissance geological map and explanatory note on the Adré sheet. Brazzaville, BRGM, 42 p.
28. Black, R., 1992. Geological Mission to Chad, January 14–February 8, 1992. UNDP/DRGM. Unpublished report, 15 p.

29. Liégeois, J.P. 1993. Measurement of Sr isotopes for the determination of the ages of magmatic rocks in Central Chad (Ouaddaï Region). Report of the Geochronology Section, Royal Museum for Central Africa, Department of Geology, 5 pp.
30. Passchier, C.W., Trouw, R.A.J., 2005.Microtectonics, 2nd, Revised and Enlarged Edition, 371p.
31. Mathieu, S., 2009. Electron Probe Microscopy. SCMEM, UHP University of Nancy1, 42 p.
32. Deer, W.A., Howie, R.A., Zussman, J., 2013. An introduction to the rock-forming minerals, 3[éme] Edition. The Mineralogical Society 507p.
33. Stüwe, K., Reif, D., Reglelsberger, E., Robl, J., Ehlers, K., Dome, J.G., 2012. Geological and mineral report of the Republic of Chad. Part 1. Spmining Survey Team of the University of Graz, Technical Report No. 7, 159 p.
34. Afiri, A., 2011. Petro-structural study of the Béni Bousera peridotites and overlying crustal rocks (Inner Rif, Morocco): Geodynamic implications. Ph.D. thesis in Earth Sciences. Cadi Ayyad University, Semlalia Faculty of Sciences, Marrakesh, Morocco. 430 pp.
35. Deer, W. A., Howie, R. A., and Zussman, J., 1966. An Introduction to the Rock-forming Minerals: Longman, London, 528 pp.
36. Miller, C.F., Sttodart, E.F., Bradfish, L.J. & Dollase, W., 1981. Composition of plutonic muscovite : genetic implications. Canadian Mineral., 19, 25-34.
37. Deer, W.A., Howie, R.A., Zussman, J.,(Eds) 1992. An introduction to the rock-forming minerals, 2nd edition. 587 Pearson Prentice Hall, 696p.
38. Guitard, G., 1970. Mesozonal Hercynian metamorphism and the eye-like gneisses of the Canigou Massif (Eastern Pyrenees). Mém. B.R.G.M., France, No. 0063, p. 1A 317.
39. Leake, B.E., Wooley, A.R., Arps, C.E.S., Birch, W.D., Gilbert, M.C., Grice, J.D., Hawthorne, F.C., Kato, A., Kisch, H.J., Krivovichev, V.G., Linthout, K., Laird, J., Mandarino, J.A., Maresch, W.V., Nickel, E.H., Rock, N.M.S., Schumacher, J.C., Smith, D.C., Stephenson, N.C.N., Ungaretti, L., Whittaker, E.J.W., Guo, Y., 1997. Nomenclature of amphiboles: report of the Subcommittee on Amphiboles of the International Mineralogical Association, Commission on New Minerals and Mineral Names. Canadian Mineralogist, 35, 219-246.
40. Léger, A., Ferry, J.M., 1991. Highly aluminos hornblende from low-pressure metacarbonates and a preliminary thermodynamic model for the Al content of calcic amphibole. American mineralogist, Volume 76, Number 5-6.
41. Morimoto, N., Fabries, J., Ferguson, A.K., Ginzburg, I.V., Ross, M., Seifert, F.A., Zussman, J., 1988. Nomenclature of pyroxenes. Mineralogical Magazine, 52, 535- 550.
42. Surour, A.A., 1995.Medium- to high-pressure garnet-amphibolites from Gebel Zabara and Wadi Sikaic south Eastern Desert, Egypt. Journal of African Earth Sciences. Vol. 21. No. 3, 443-457.
43. Ding, L., Dalai, Zhong.,An, Yin., Paul Kapp., T. Mark, Harrison., 2001. Cenozoic structural and metamorphic evolution of the eastern Himalayan syntaxis (Namche Barwa). Earth and Planetary Science Letters. Volume 192, Issue 3, Pages 423-438.
44. Isseini, M., André-Mayer, A.-S., Vanderhaeghe, O., Barbey, P., Deloule, E., 2012. A-type granites from the Pan-African orogenic belt in south-western Chad constrained using geochemistry, Sr–Nd isotopes and U–Pb geochronology. Lithos 153, 39-52.
45. Caby, R., Bertrand, J.M.L., and Black, R., 1981. Closure of the Pan-African Ocean and continental collision in the Hoggar-Iforas segment, in the central Sahara. In Precambrian plate tectonics. Edited by A. Kröner. Elsevier, Amsterdam, Netherlands, pp. 407–434.
46. Caby, R., and Andreopoulos-Renaud, U., 1987. The Eastern Hoggar, a cratonized block dating to 730 Ma in the Pan-African orogen of northern Africa. Precambrian Research, 36 : 335–344.
47. Liégeois, J.P., Bertrand, J.M., and Black, R., 1987. The subduction and collision-related Pan-African composite batholith of the Adrar des Iforas (Mali): a review. Geological Journal, 22: 185–211.
48. Toteu, S.F., Van Schmus, W.R., Penaye, J., Nyobe, J.B., 1994.U-Pb and Sm-Nd evidence for Eburnean and Pan-African high-grade metamorphism in cratonic rocks of Southern Cameroon. Precambrian Res. 67, 321–347.
49. Bouyo Houketchang, M., Zhao, Y., Penaye, J., Zhang, S.H., Njel, U.O., 2015. Neoproterozoic subduction-related metavolcanic and metasedimentary rocks from the Rey Bouba greenstone belt in north-central Cameroon, within the Central African Fold Belt: new insights into a continental arc geodynamic setting. Precambrian Res. 261, 40–53.
50. El-Makhrouf, A.A., 1988. Tectonic interpretation of Jebel Eghei area and its regional application to Tibesti orogenic belt, south central Libya (S.P.L.A.J). Journal of African Earth Sciences 7, 645–967.
51. Kasser, M.Y., 1995. Precambrian evolution of the Mayo Kebbi region (Chad). A segment of the Pan-African Chain. Third Cycle Doctorate, Natural History Museum of Paris (France), 217 p.
52. Pin, C., Poidevin, J.L., 1987. U-Pb Zircon evidence for a Pan-African granulite facies metamorphism in the Central African Republic: A new interpretation of the high-grade series of the northern border of the Congo craton, Precambrian Res., 36, 303–312.

53. Malik, H.M., NgonNgon, G.F., Vishiti, A., André Mayer, A-S., Isseini, M., Djerossem, F., Al-Gadam, I.O., 2024. Petrography and mineral microchemical signature of lode gold mineralization in Goz-Beida, southern Ouaddaï massif, eastern Chad. Arabian Journal of Geosciences. 17:207. https://doi.org/10.1007/s12517-024-12011-5.
54. Djerossem, F.N., Rirabé, N., Baïssemia, G.R., Klamadji, M.N., Malik, H.M., 2024.Lineament and Lithological Mapping of Meta-Sediments and Granitoids of Goz-Beïda (Eastern Chad) Based on Semi-Automatic Processing of Landsat 8 Oli/Tirs Images.Journal of Geosciences and Geomatics, 2024, Vol. 12, No. 4, 80-86.